The European Physical Journal Special Topics manuscript No.
(will be inserted by the editor)

Analysing Complex Dynamics of Mandelbrot and Julia Sets Generated using Picard–SP Iteration Scheme

Bashir Nawaz[1] · **Krzysztof Gdawiec**[2] · **Kifayat Ullah**[1]

Received: ... / Accepted: ...

Abstract One of the generalizations of Mandelbrot and Julia sets introduced in the literature involves using iteration schemes from fixed-point theory to generate new classes of these sets. In this article, we propose employing the Picard–SP iteration to define a new class of Mandelbrot and Julia sets for polynomials of the form $x^{k+1} + c$, where $x, c \in \mathbb{C}$ and $k \geq 1$. We formulate an escape criterion to generate complex graphics of the considered class of sets. Our analysis covers dynamic variations, generation timelines, shapes and colours of the resulting visuals. Furthermore, we inspect the impact of iteration parameters on Mandelbrot and Julia sets using established numerical measures from the existing literature. The results show that the sets obtained with the Picard–SP iteration are very complex, and the variation of the iteration's parameters has a significant impact on the sets. Moreover, the dependency between the parameters and the numerical measures is non-trivial and non-linear.

Keywords Mandelbrot set · Julia set · Picard–SP iteration · escape criterion

Bashir Nawaz
E-mail: bashirnawaz.482@gmail.com ORCID: 0009-0006-5089-2539

Krzysztof Gdawiec (✉)
E-mail: krzysztof.gdawiec@us.edu.pl ORCID: 0000-0001-9434-9307

Kifayat Ullah
E-mail: kifayatmath@yahoo.com

[1] Department of Mathematics, University of Lakki Marwat, Lakki Marwat 28420, Khyber Pakhtunkhwa, Pakistan
[2] Institute of Computer Science, University of Silesia in Katowice, Bedzinska 39, 41-200, Sosnowiec, Poland

1 Introduction

Fractal geometry offers a comprehensive framework to study complex and irregular shapes found in nature, such as coastlines, mountains, clouds, trees and branches, rivers and streams [12]. Fractals are also shapes with irregular structures that cannot be expressed using Euclidean geometry [11]. A fractal can be described as a mathematical shape where each point displays the identical structure as the whole. Some of the most notable examples of fractals in fractal geometry include the Mandelbrot and Julia sets.

Pierre Fatou and Gaston Julia tried to iterate the function $x \to x^2 + c$ where $x, c \in \mathbb{C}$. Julia [14] successfully iterated the function $x \to x^2 + c$ but was unsuccessful in depicting it visually. Benoit Mandelbrot [21] successfully plotted the graph for this type of function. In the Julia set, we inspect how the iterates perform for each x, while in the Mandelbrot set, we explore the connectedness of the Julia set corresponding to the parameter c that outlines these sets. In [19], the authors generalized the concept of Mandelbrot sets by substituting the quadratic function $x \to x^2 + c$ with $x \to x^k + c$, where $k \geq 2$.

Fixed point theory is an effective tool in mathematics for studying nonlinear natural phenomena such as analysing population models in population dynamics [3], finding equilibrium points for demand and supply in economics equilibrium [8], ecological models in ecological systems to understand the interaction between the species [7], etc. In fixed point theory, iteration processes are designed to approximate fixed points of the specific mappings. Some of these iterations processes are Mann [22], Ishikawa [13], Agarwal [2], Noor [27], M [34], etc. This branch is also recognized as the most potent tool for creating fractals.

Rani et al. [30,31], generated the so-called superior Julia and Mandelbrot sets using Mann iteration process. In [29], the authors explored relative superior Julia and Mandelbrot sets using the Ishikawa iteration process. Later, other one-step iteration proccess were studied. For example, Zou et al. in [36] proposed the Picard–Mann and Nawaz et al. in [25] the M-iteration process to study the properties of the Mandelbrot and Julia sets. In [5], Ashish et al. generated Julia and Mandelbrot sets using a three-step Noor iteration process. In the literature, we can also find the use of implicit iteration processes. For example, in [20], the Jungck–Mann iteration was used to generate Julia sets, and in [32], the Jungck–Noor implicit scheme was used to obtain Mandelbrot and Julia sets images. Moreover, the implicit iteration schemes were extended with s-convexity. For example, the Jungck–Mann iteration with s-convexity was introduced to generate Mandelbrot and Julia sets in [33], and in [4] the Jungck–Ishikawa iteration with s-convexity was used to obtain some variants of Mandelbrot and Julia sets. The viscosity-type of iteration processes is the next group recently used in the generation of complex fractals. Three such applications can be found in [18,17,23]. Recently, the idea of using iteration schemes from the fixed point theory in the generation of the quaternion Julia sets was introduced. In [10], Gdawiec et al. used the Picard–Mann iteration for this kind of set.

Leveraging the innovative approach of fixed point theory, this paper presents a generalization of Mandelbrot and Julia sets. Specifically, we introduce, for the first time, the use of the Picard–SP orbit, a recently developed iteration scheme by Nawaz et al. [24], in the generation of these iconic fractal structures. This novel application of the Picard–SP orbit represents a significant departure from traditional iteration methods. It defines a new dynamical system and enables the creation of entirely new and diverse geometric shapes for both Mandelbrot and Julia sets.

To achieve these results, we rigorously establish the escape criterion for the function $x^{k+1} + c$ when iterated under the Picard–SP scheme. This criterion serves as the foundational mathematical framework for our exploration, ensuring the accurate and reliable generation of the sets. Furthermore, we provide a comprehensive collection of graphical illustrations to demonstrate the unique and intricate patterns that arise from our proposed approach. Beyond the visual and theoretical advancements, we delve into an in-depth quantitative analysis of how the parameters of the iteration influence key numerical measures associated with these fractal sets. Drawing on methodologies outlined in [17], we highlight the intricate interplay between parameter selection and fractal properties, offering new insights into the dynamical behaviour of these systems.

In sum, this work not only broadens the scope of fractal geometry through the introduction of a novel dynamical system but also lays the groundwork for future investigations into the mathematical and aesthetic complexities of Mandelbrot and Julia sets.

The rest of the paper is organized as follows. Section 2 highlights some essential definitions and facts required for subsequent discussions. Section 3 establishes the escape criterion for the function and iteration scheme under consideration. Section 4 showcases graphical images of Mandelbrot and Julia sets generated in Picard–SP orbit. Section 5 examines the relationships between the iteration's parameters and numerical measures. Finally, Section 6 offers concluding remarks on the study.

2 Preliminaries

In this section, we introduce some definitions and facts needed in the rest of the paper.

Definition 1 (Julia set [35]) Let $q_c : \mathbb{C} \to \mathbb{C}$ be a complex polynomial function with a parameter $c \in \mathbb{C}$. The filled Julia set is defined as

$$J_{q_c} = \{x \in \mathbb{C} : \{|q_c^n(x)|\}_{n=0}^{\infty} \text{ is bounded}\},$$

where q_c^n represents the nth iterate of the function q_c. The boundary of J_{q_c} is called the Julia set.

Definition 2 (Mandelbrot set [9]) The Mandelbrot set includes all values of c for which the filled Julia set J_{q_c} is connected, i.e.,

$$M = \{c \in \mathbb{C} : J_{q_c} \text{ is connected}\}.$$

Remark 1 Equivalently, the Mandelbrot set can be defined as [35]

$$M = \{c \in \mathbb{C} : |q_c^n(\eta)| \nrightarrow \infty \text{ as } n \to \infty\},$$

where η is a critical point of q_c, i.e, $q_c'(\eta) = 0$.

Definition 3 Let $T : X \to X$ be a mapping, and let us take $x_0 \in X$. We call the sequence $\{x_n\}$ defined as

$$\begin{aligned} v_n &= (1-\gamma_n)x_n + \gamma_n T x_n, \\ y_n &= (1-\beta_n)v_n + \beta_n T v_n, \\ w_n &= (1-\alpha_n)y_n + \alpha_n T y_n, \\ x_{n+1} &= T w_n. \end{aligned} \tag{1}$$

where $\alpha_n, \beta_n, \gamma_n \in [0,1]$ for all $n \in \mathbb{N}$, the Picard–SP orbit of x_0 [24].

Remark 2 We can notice from (1) that

- If $\gamma_n = 0$ for all $n \in \mathbb{N}$, then (1) is transformed into the Picard normal S orbit [15]

$$\begin{aligned} y_n &= (1-\beta_n)x_n + \beta_n T x_n, \\ w_n &= (1-\alpha_n)y_n + \alpha_n T y_n, \\ x_{n+1} &= T w_n. \end{aligned} \tag{2}$$

- If $\beta_n = \gamma_n = 0$ for all $n \in \mathbb{N}$, then (1) is transformed into the Picard–Mann orbit [16]

$$\begin{aligned} w_n &= (1-\alpha_n)x_n + \alpha_n T x_n \\ x_{n+1} &= T w_n. \end{aligned} \tag{3}$$

- If $\alpha_n = \beta_n = \gamma_n = 0$ for all $n \in \mathbb{N}$, then (1) represents the Picard orbit [28]

$$x_{n+1} = T w_n. \tag{4}$$

In the rest of the paper, we assume constant sequences of the iterations' parameters, i.e., $\alpha_n = \alpha$, $\beta_n = \beta$, $\gamma_n = \gamma$, where $\alpha, \beta, \gamma \in (0,1]$.

3 Escape criterion for the Picard–SP iteration

In this section, we derive the escape criterion, which serves as the important component in the escape-time algorithm employed for creating the Mandelbrot and Julia sets. Let $x_0 \in \mathbb{C}$ and $q_c(x) = x^{k+1} + c$. We consider the following Picard–SP orbit

$$\begin{aligned} v_n &= (1-\gamma)x_n + \gamma q_c(x_n), \\ y_n &= (1-\beta)v_n + \beta q_c(v_n), \\ w_n &= (1-\alpha)y_n + \alpha q_c(y_n), \\ x_{n+1} &= q_c(w_n), \end{aligned} \tag{5}$$

where $\alpha, \beta, \gamma \in (0, 1]$.

Now, we can consider conditions under which the orbit of the Picard–SP iteration for a given starting point escapes to infinity.

Theorem 1 *Let $q_c(x) = x^{k+1} + c$, where $c \in \mathbb{C}$ and $k = 1, 2, 3, \ldots$. Assume that $x_0 \in \mathbb{C}$ and*

$$|x_0| \geq |c|, \tag{6}$$

$$|x_0| > \left(\frac{2}{\gamma}\right)^{\frac{1}{k}}, |x_0| > \left(\frac{2}{\beta}\right)^{\frac{1}{k}}, |x_0| > \left(\frac{2}{\alpha}\right)^{\frac{1}{k}}, \tag{7}$$

where $\alpha, \beta, \gamma \in (0, 1]$. Then, $|x_n| \to \infty$ as $n \to \infty$, where x_n is defined in (5).

Proof For $n = 0$, consider

$$|v_0| = |(1-\gamma)x_0 + \gamma q_c(x_0)|.$$

As $q_c(x_0) = x_0^{k+1} + c$, we get

$$\begin{aligned} |v_0| &= |(1-\gamma)x_0 + \gamma(x_0^{k+1} + c)| \\ &= |\gamma x_0^{k+1} + (1-\gamma)x_0 + \gamma c| \\ &\geq \gamma|x_0^{k+1}| - (1-\gamma)|x_0| - \gamma|c| \\ &\geq \gamma|x_0^{k+1}| - (1-\gamma)|x_0| - \gamma|x_0| \ \because |x_0| \geq |c| \\ &= \gamma|x_0^{k+1}| - |x_0| + \gamma|x_0| - \gamma|x_0| \\ &\geq |x_0|(\gamma|x_0|^k - 1). \end{aligned}$$

Hence,

$$|v_0| \geq |x_0|(\gamma|x_0|^k - 1). \tag{8}$$

Now, in the second step of the Picard–SP orbit

$$|y_0| = |(1-\beta)v_0 + \beta q_c(v_0)| = |(1-\beta)v_0 + \beta(v_0^{k+1} + c)|. \tag{9}$$

Using (8) in (9), we get

$$|y_0| \geq \left|(1-\beta)|x_0|(\gamma|x_0|^k - 1) + \beta(|x_0|^{k+1}(\gamma|x_0|^k - 1)^{k+1} + c)\right|. \tag{10}$$

Since $|x_0| > \left(\frac{2}{\gamma}\right)^{\frac{1}{k}}$, we obtain

$$\begin{aligned} \gamma|x_0|^k &> 2 \\ \gamma|x_0|^k - 1 &> 1 \\ |x_0|(\gamma|x_0|^k - 1) &> |x_0| \\ |x_0|^{k+1}(\gamma|x_0|^k - 1)^{k+1} &> |x_0|^{k+1}. \end{aligned} \tag{11}$$

Using (11) in (10), we obtain

$$\begin{aligned} |y_0| &\geq |(1-\beta)|x_0| + \beta(|x_0|^{k+1} + c)| \\ &= \left|\beta|x_0|^{k+1} + (1-\beta)|x_0| + \beta c\right| \\ &\geq \beta|x_0|^{k+1} - (1-\beta)|x_0| - \beta|c| \\ &\geq \beta|x_0|^{k+1} - (1-\beta)|x_0| - \beta|x_0| \ \ \because |x_0| \geq |c| \\ &= \beta|x_0|^{k+1} - |x_0| \\ &= |x_0|(\beta|x_0|^k - 1). \end{aligned} \tag{12}$$

Hence,

$$|y_0| \geq |x_0|(\beta|x_0|^k - 1). \tag{13}$$

In the third step of the Picard–SP orbit, we have

$$\begin{aligned} |w_0| &= |(1-\alpha)y_0 + \alpha q_c(y_0)| \\ &= |(1-\alpha)y_0 + \alpha(y_0^{k+1} + c)|. \end{aligned} \tag{14}$$

Using (13) in (14), we obtain

$$|w_0| \geq \left|(1-\alpha)|x_0|(\beta|x_0|^k - 1) + \alpha(|x_0|^{k+1}(\beta|x_0|^k - 1)^{k+1} + c)\right|. \tag{15}$$

From the assumption $|x_0| > \left(\frac{2}{\beta}\right)^{\frac{1}{k}}$, we get $\beta|x_0|^k - 1 > 1$ and $|x_0|^{k+1}(\beta|x_0|^k - 1)^{k+1} > |x_0|^{k+1}$. Using this in (15), we get

$$\begin{aligned} |w_0| &\geq \left|(1-\alpha)|x_0| + \alpha(|x_0|^{k+1} + c)\right| \\ &= \left|\alpha|x_0|^{k+1} + (1-\alpha)|x_0| + \alpha c\right| \\ &\geq \alpha|x_0|^{k+1} - (1-\alpha)|x_0| - \alpha|c| \\ &\geq \alpha|x_0|^{k+1} - |x_0| + \alpha|x_0| - \alpha|x_0| \ \ \because |x_0| \geq |c| \\ &= \alpha|x_0|(\alpha|x_0|^k - 1). \end{aligned}$$

Hence,

$$|w_0| \geq |x_0|(\alpha|x_0|^k - 1). \tag{16}$$

In the fourth step of the Picard–SP orbit, we get

$$|x_1| = |q_c(w_0)| = |w_0^{k+1} + c|. \tag{17}$$

Now,

$$\begin{aligned} |x_1| &= |w_0^{k+1} + c| \\ &\geq |w_0|^{k+1} - |c| \\ &\geq |w_0|^{k+1} - |x_0| \ \ \because |x_0| \geq |c|. \end{aligned} \tag{18}$$

Using (16), we have

$$|x_1| \geq ||x_0|(\alpha|x_0|^k - 1)|^{k+1} - |x_0| \tag{19}$$

Since $|x_0| > \left(\frac{2}{\alpha}\right)^{\frac{1}{k}}$, we obtain

$$\begin{aligned} \alpha|x_0|^k &> 2 \\ \alpha|x_0|^k - 1 &> 1 \\ (\alpha|x_0|^k - 1)^{k+1} &> 1 \\ |x_0|^{k+1}(\alpha|x_0| - 1)^{k+1} &> |x_0|^{k+1}. \end{aligned} \tag{20}$$

Using (20) in (19), we get

$$|x_1| \geq |x_0|^{k+1} - |x_0| = |x_0|(|x_0|^k - 1). \tag{21}$$

Because $|x_0| > \left(\frac{2}{\alpha}\right)^{\frac{1}{k}} > 2^{\frac{1}{k}}$, we get $|x_0|^k - 1 > 1$. Therefore, there exists $\eta > 0$ such that $|x_0|^k - 1 > 1 + \eta > 1$. As a result, we obtain

$$|x_1| > |x_0|(1 + \eta).$$

Since $|x_1| \geq |x_0|$, we may apply the same arguments repeatedly to obtain

$$\begin{aligned} |x_2| &> |x_0|(1+\eta)^2, \\ |x_3| &> |x_0|(1+\eta)^3, \\ &\vdots \\ |x_n| &> |x_0|(1+\eta)^n. \end{aligned}$$

Hence $|x_n| \to \infty$ as $n \to \infty$. □

From Theorem 1, we obtain the following two important corollaries.

Corollary 1 *Let $q_c(x) = x^{k+1} + c$, $k = 1, 2, 3, \ldots$ and $c \in \mathbb{C}$. Suppose that*

$$|x_0| > \max\left\{|c|, \left(\frac{2}{\alpha}\right)^{\frac{1}{k}}, \left(\frac{2}{\beta}\right)^{\frac{1}{k}}, \left(\frac{2}{\gamma}\right)^{\frac{1}{k}}\right\}. \tag{22}$$

Then, for x_n defined by (5), we have $|x_n| \to \infty$ as $n \to \infty$.

Corollary 2 *Let $q_c(x) = x^{k+1} + c$, where $c \in \mathbb{C}$ and $k = 1, 2, 3, \ldots$. Suppose that for x_n defined in (5), we have*

$$|x_j| > \max\left\{|c|, \left(\frac{2}{\alpha}\right)^{\frac{1}{k}}, \left(\frac{2}{\beta}\right)^{\frac{1}{k}}, \left(\frac{2}{\gamma}\right)^{\frac{1}{k}}\right\} \tag{23}$$

for some $j \geq 0$. Then, there exists $\eta > 0$ such that $|x_{n+j}| > |x_j|(1+\eta)^n$, and we have $|x_n| \to \infty$ as $n \to \infty$.

The condition in (23) is called the escape criterion, and is the base for the escape-time algorithm to generate Mandelbrot and Julia sets for the Picard–SP iteration.

4 Graphical Examples

In this section, we present graphical examples of the Mandelbrot and Julia sets generated using the Picard–SP iteration with various parameter settings.

4.1 Graphical Examples of Mandelbrot Sets

To generate the images of the Mandelbrot set using Piacrd–SP iteration, we used the escape-time algorithm, which uses the escape criterion derived in Sec. 3. Algorithm 1 presents the pseudocode of this algorithm. The algorithm employs two bounds to terminate the while loop. The first bound, $|x_n| \leq R$, directly applies the escape criterion derived in Sec. 3. This condition ensures that the loop stops when the escape criterion is satisfied, indicating that the orbit will diverge to infinity. However, for non-escaping points, the condition $|x_n| \leq R$ is never satisfied for any n. In such cases, the algorithm would otherwise continue indefinitely, resulting in an infinite loop. To prevent this, we impose a second bound by limiting the maximum number of iterations to K. This means that if the algorithm reaches K iterations without meeting the escape condition, the point is assumed to be non-escaping. Consequently, the second bound is defined as $n \leq K$.

4.1.1 Quadratic Mandelbrot Sets ($k = 1$)

For the quadratic Mandelbrot set examples ($k = 1$), we used the following common parameters: $K = 25$, $A = [-2.5, 2.5]^2$, and a colour map given in Fig. 1.

Because the Picard–SP iteration has three parameters (α, β, γ), we divide each example into three figures. We fix two out of the three parameters in each figure and vary the remaining one. Figures 2–4 show images generated with Algorithm 1, for varying α, β, and γ, respectively. In each figure, we can observe that the iteration's parameters have a significant impact on the size and shape of the set. The set becomes larger with the decrease of each of

Algorithm 1: Mandelbrot set generation

Input: $q_c(x) = x^{k+1} + c$, where $c \in \mathbb{C}$ and $k = 1, 2, \ldots$; $A \subset \mathbb{C}$ – area; K – the maximum number of iterations; $\alpha, \beta, \gamma \in (0, 1]$ – parameter for the Picard–SP iteration; $colourmap[0..C-1]$ – colour map with C colours.

Output: Mandelbrot set for area A.

for $c \in A$ **do**
- $R = \max\left\{|c|, \left(\frac{2}{\alpha}\right)^{\frac{1}{k}}, \left(\frac{2}{\beta}\right)^{\frac{1}{k}}, \left(\frac{2}{\gamma}\right)^{\frac{1}{k}}\right\}$
- $n = 0$
- $x_0 = 0$
- **while** $|x_n| \leq R$ **and** $n \leq K$ **do**
  - $v = (1-\gamma)x_n + \gamma q_c(x_n)$
  - $y = (1-\beta)v + \beta q_c(v)$
  - $w = (1-\alpha)y + \alpha q_c(y)$
  - $x_{n+1} = q_c(w)$
  - $n = n + 1$
- $i = \left\lfloor (C-1)\frac{n}{K} \right\rfloor$
- colour c with $colourmap[i]$

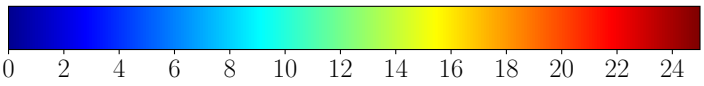

Fig. 1 Color map used in the graphical examples

the three parameters. However, the shape changes are different in each case. Moreover, it can be seen that quadratic Mandelbrot sets exhibit symmetrical behaviour along the real axis.

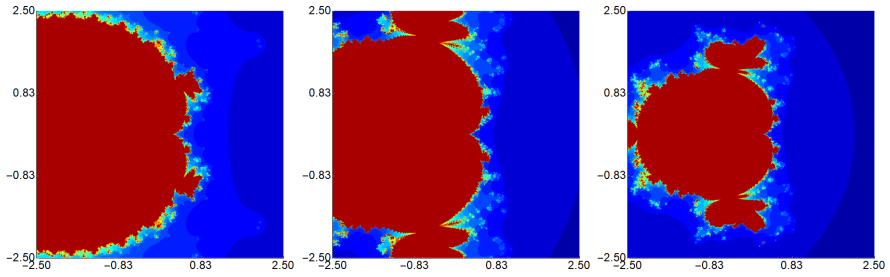

(a) $\alpha = 0.05$ (b) $\alpha = 0.55$ (c) $\alpha = 0.95$

Fig. 2 Quadratic Mandelbrot sets ($k = 1$) generated using Picard–SP iteration for $\beta = 0.45$, $\gamma = 0.15$, and varying α

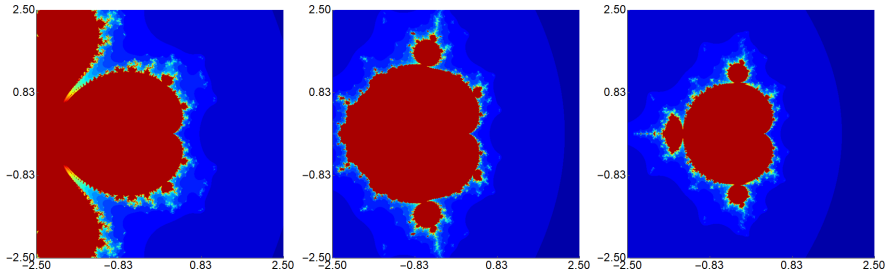

(a) $\beta = 0.17$ (b) $\beta = 0.42$ (c) $\beta = 0.72$

Fig. 3 Quadratic Mandelbrot sets ($k = 1$) generated using Picard–SP iteration for $\alpha = 0.10$, $\gamma = 0.80$, and varying β

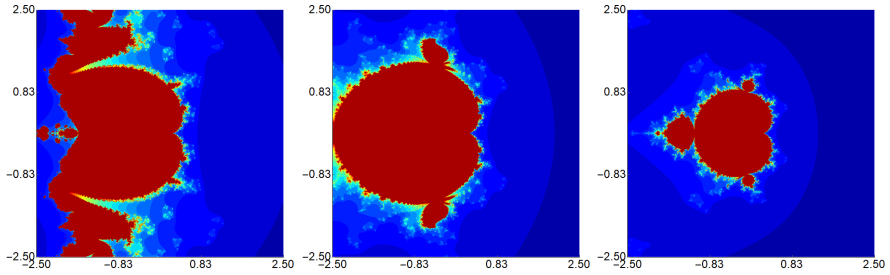

(a) $\gamma = 0.17$ (b) $\gamma = 0.47$ (c) $\gamma = 0.91$

Fig. 4 Quadratic Mandelbrot sets ($k = 1$) generated using Picard–SP iteration for $\alpha = 0.86$, $\beta = 0.16$, and varying γ

4.1.2 Quartic Mandelbrot Sets ($k = 3$)

For the quartic Mandelbrot set, we used the following common parameters: $K = 25$, $A = [-2, 2]^2$, and the same colour map as we used for the quadratic Mandelbrot sets. The images shown in Figs. 5–7 are obtained by varying values of α, β and γ parameters, respectively. In this example, we can observe that the parameters have a smaller impact on the size and shape of the generated sets than in the case of the quadratic sets. The biggest size change can be seen for the varying α parameter, and the smallest change for the γ parameter. In each case, the lower the value of the varying parameter, the larger the set. In the images, we can also see variations in shapes. The largest shape changes can be observed when we vary the γ parameter. Moreover, in each image, we see that the generated sets have 3-fold rotational symmetry.

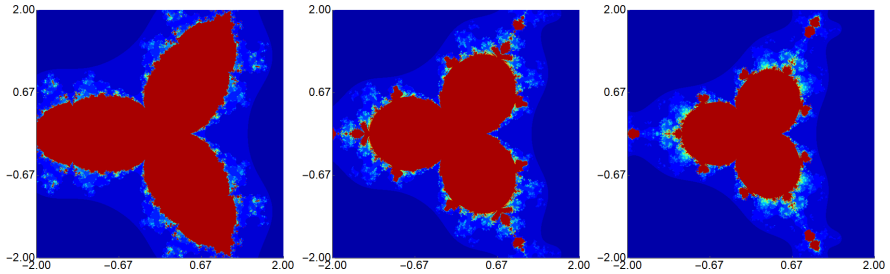

(a) $\alpha = 0.20$ (b) $\alpha = 0.48$ (c) $\alpha = 0.86$

Fig. 5 Quartic Mandelbrot ($k = 3$) sets in Picard–SP iteration for $\beta = 0.55$, $\gamma = 0.10$, and varying α

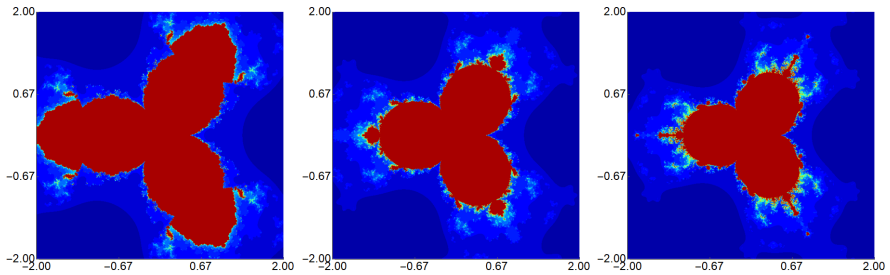

(a) $\beta = 0.25$ (b) $\beta = 0.64$ (c) $\beta = 0.93$

Fig. 6 Quartic Mandelbrot sets in Picard-SP iteration for $\alpha = 0.10$, $\gamma = 0.55$, and varying β

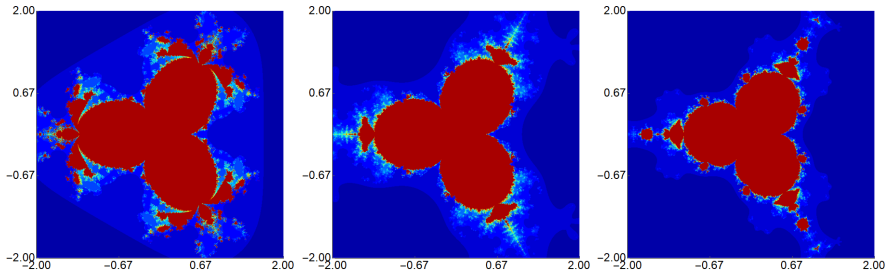

(a) $\gamma = 0.05$ (b) $\gamma = 0.57$ (c) $\gamma = 0.91$

Fig. 7 Quartic Mandelbrot sets in Picard-SP iteration for $\alpha = 0.60$, $\beta = 0.15$, and varying γ

4.2 Graphical Examples of Julia Sets

In this section, we generate quadratic and quartic Julia sets using the Picard–SP iteration, applying the proven escape criterion. Algorithm 2 presents the pseudocode for the escape-time algorithm used in this process. The algorithm utilizes the escape criterion in a manner identical to that of the Mandelbrot set generation algorithm. Additionally, we implement the same measures to prevent an infinite loop for non-escaping points.

Algorithm 2: Julia set generation

Input: $q_c(x) = x^{k+1} + c$, where $k = 1, 2, \ldots$; $c \in \mathbb{C}$ – parameter; $A \subset \mathbb{C}$ – area; K – the maximum number of iterations; $\alpha, \beta, \gamma \in (0, 1]$ – parameters for the Picard–SP iteration; $colourmap[0..C-1]$ – colour map with C colours.
Output: Julia set for area A.

$R = \max\left\{|c|, \left(\frac{2}{\alpha}\right)^{\frac{1}{k}}, \left(\frac{2}{\beta}\right)^{\frac{1}{k}}, \left(\frac{2}{\gamma}\right)^{\frac{1}{k}}\right\}$
for $x_0 \in A$ **do**
  $n = 0$
  while $|x_n| \leq R$ **and** $n \leq K$ **do**
    $v = (1-\gamma)x_n + \gamma q_c(x_n)$
    $y = (1-\beta)v + \beta q_c(v)$
    $w = (1-\alpha)y + \alpha q_c(y)$
    $x_{n+1} = q_c(w)$
    $n = n + 1$
  $i = \lfloor (C-1)\frac{n}{K} \rfloor$
  colour c with $colourmap[i]$

4.2.1 Quadratic Julia Sets ($k = 1$)

We generated images of quadratic Julia sets for the Picard–SP iteration using the following common parameters: $K = 25$, $A = [-2, 2]^2$, $c = -2.20$, and the colour map shown in Fig. 1. As in the case of quadratic Julia sets, we divided the images into three figures. In each figure, we fix two of the three parameters and vary the remaining one. The images generated with the mentioned values of the common parameters are presented in Figs. 8–10. In each case, we see that the iteration's parameters (α, β, γ) have a significant impact on the size of the generated set. The most significant changes are observed for the varying α parameter. For each varying parameter, we see that the sets become larger with the decrease of the parameter. The shapes of the sets also changed, and the changes were different for each parameter. In all cases, the generated sets exhibit axial symmetry, with the real line serving as the axis of symmetry.

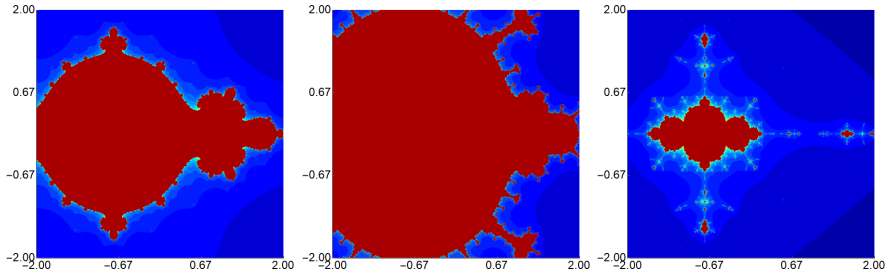

(a) $\alpha = 0.01$ (b) $\alpha = 0.11$ (c) $\alpha = 0.95$

Fig. 8 Quadratic Julia sets in Picard–SP orbit for different $\beta = 0.01$, $\gamma = 0.4$, and varying α

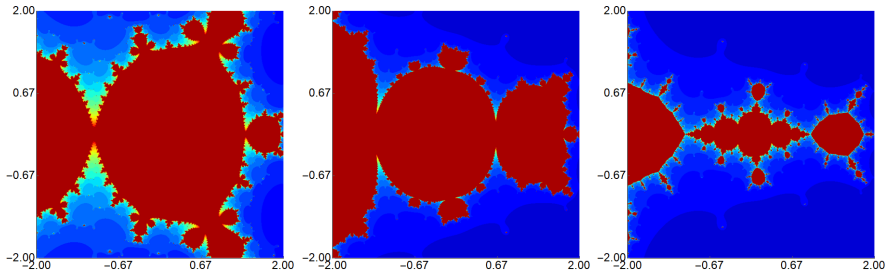

(a) $\beta = 0.05$ (b) $\beta = 0.55$ (c) $\beta = 0.76$

Fig. 9 Quadratic Julia sets in Picard–SP orbit for $\alpha = 0.03$, $\gamma = 0.10$, and varying β

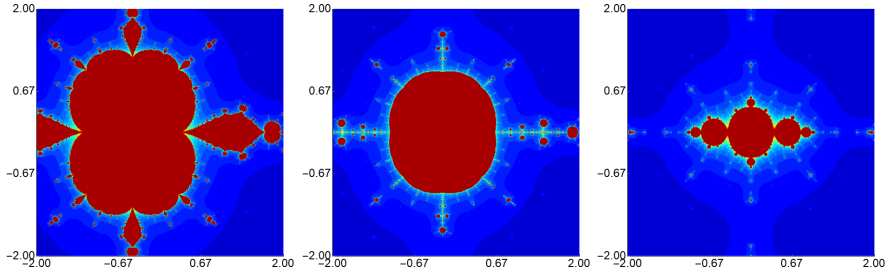

(a) $\gamma = 0.53$ (b) $\gamma = 0.7$ (c) $\gamma = 1.0$

Fig. 10 Quadratic Julia sets in Picard–SP orbit for $\alpha = 0.02$, $\beta = 0.10$, and varying γ

4.2.2 Quartic Julia Sets ($k = 3$)

For the quartic Julia sets, we used the following common parameters: $K = 25$, $A = [-2.5, 2.5]^2$, $c = -0.8 - 0.1i$, and the colour map in Fig. 1. Among the examples presented, the shape variations are the most pronounced, differing

significantly for each varying parameter. While the size of the sets also changes, these variations are relatively small. Furthermore, most of the generated images lack axial or rotational symmetry, as certain areas disrupt the symmetry.

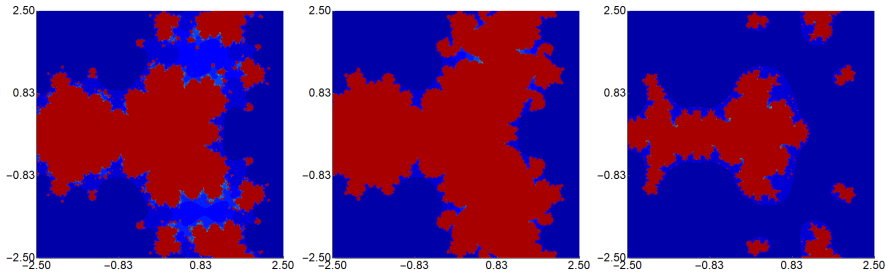

(a) $\alpha = 0.045$ (b) $\alpha = 0.093$ (c) $\alpha = 1.0$

Fig. 11 Quartic Julia sets in Picard–SP orbit for $\beta = 0.064$, $\gamma = 0.04$, and varying α

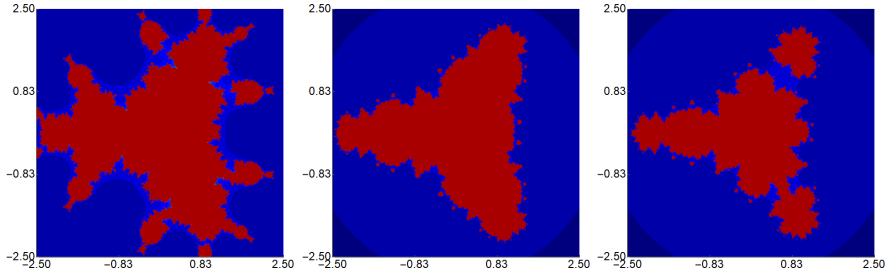

(a) $\beta = 0.01$ (b) $\beta = 0.54$ (c) $\beta = 0.94$

Fig. 12 Quartic Julia sets in Picard–SP orbit for $\alpha = 0.08$, $\gamma = 0.10$, and varying β

5 Numerical Results

We can notice from Sec. 4 that the geometry and size of the Mandelbrot and Julia sets generated via the Picard–SP iteration are affected by the values of iteration's parameters α, β, and γ. It is quite interesting to study how these iteration parameters relate to the shapes and sizes of the sets. We can use two numerical measures introduced in [17] to study such a behaviour. The first measure, the average escape time (AET), gives us information on the average number of iterations performed only for the escaping points. The second measure, the non-escaping area index (NAI), is a number from $[0, 1]$

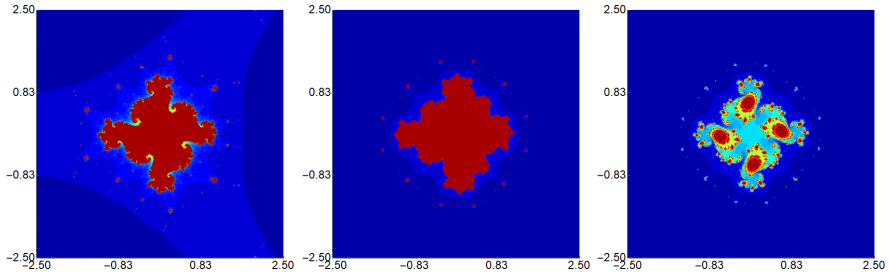

(a) $\gamma = 0.001$ (b) $\gamma = 0.8$ (c) $\gamma = 1.0$

Fig. 13 Quartic Julia sets in Picard–SP orbit for $\alpha = 0.01$, $\beta = 0.02$, and varying γ

that indicates the percentage of the considered area covered by non-escaping points (points for which we perform the maximum of K iterations), so it is a relative set size in the considered area.

In the subsequent sections, we investigate the dependency between Picard–SP iteration parameters and AET, NAI numerical measures for the Mandelbrot and Julia sets. Because Picard-SP iteration has three parameters, i.e., α, β, and γ, so it is not possible for us to present the results by varying all three parameters at once in a clear way. Therefore, to resolve this issue, we present several 2D cross-sections in which we fix the value of γ and vary α and β parameters. The α and β parameters are changed using the step size of 0.01. Consequently, $10,000$ images are generated for a single heat map.

In the experiments, we need to generate a large number of images ($10,000$ per plot), so the entire generation process is time-consuming. To get a reasonable time of the experiments, we can use various approaches. Because each point in the escape-time algorithms (Algorithm 1 and 2) is processed independently, so we can use parallelization of the computations obtained with the use of multicore processors or computations on the graphics processing unit. Moreover, we can reduce the maximal number of iterations K, for example, to 25 iterations. For larger values of K, the approximation of Mandelbrot and filled Julia sets (points for which we perform K iterations) shown in the images differs only by several pixels, but the time is significantly longer than for $K = 25$.

In our experiments, the image generation algorithms were implemented in Mathematica 11.3, utilizing the parallelization feature of the `Compile` command, with images produced at a resolution of 800×800 pixels. The numerical experiments were conducted on a computer system featuring an Intel i5–1235U processor running at 1.3 GHz and Windows 10 (64-bit).

5.1 Numerical Results for Mandelbrot Sets

For the numerical experiments involving the Mandelbrot set, we used the same value of K and the same area A as for the Mandelbrot sets presented in Sec. 4.1.

In our first experiment, for the quadratic Mandelbrot set, we used the following values of γ to obtain our results: 0.1, 0.4, 0.7, 1.0. The obtained results are shown in Figs. 14–15, and the maximal and minimal values of AET and NAI are given in Tab. 1.

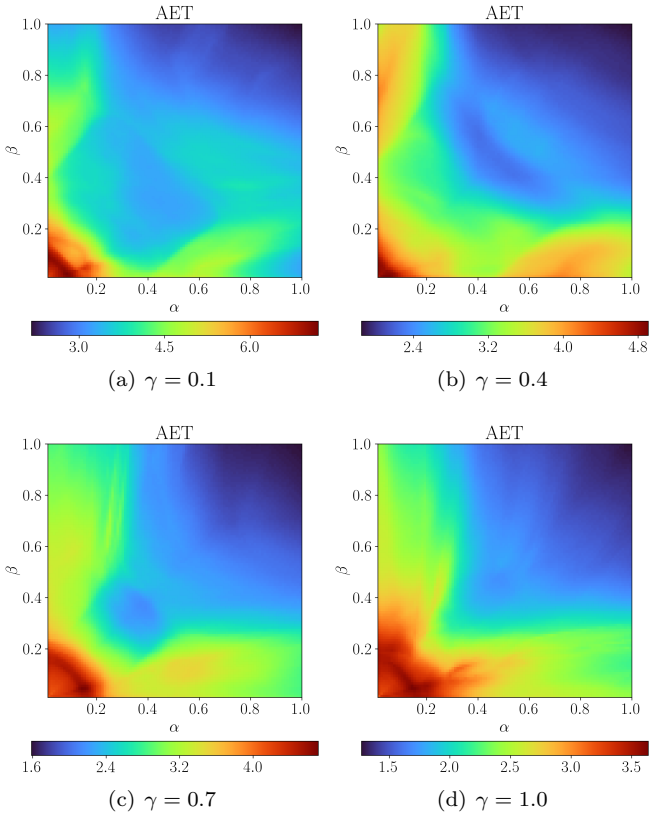

(a) $\gamma = 0.1$ (b) $\gamma = 0.4$

(c) $\gamma = 0.7$ (d) $\gamma = 1.0$

Fig. 14 2D cross-sections of AET for quadratic Mandelbrot set – varying α, β and fixed γ

When examining the AET plots, we can notice a gradual decrease in AET values with the increase in values of the γ parameter. The highest AET value (7.195) is attained for $\gamma = 0.1$ at $\alpha = 0.08$, $\beta = 0.02$. The high AET value indicates that points remained bounded for many iterations before escaping. Similarly, the lowest AET value (1.27) is obtained for $\gamma = 1.0$ at $\alpha = \beta = 1.0$. For all cross-sections, we see that the dependency is non-linear and that the concentration of high values of AET is located in the lower-left corner, i.e., for

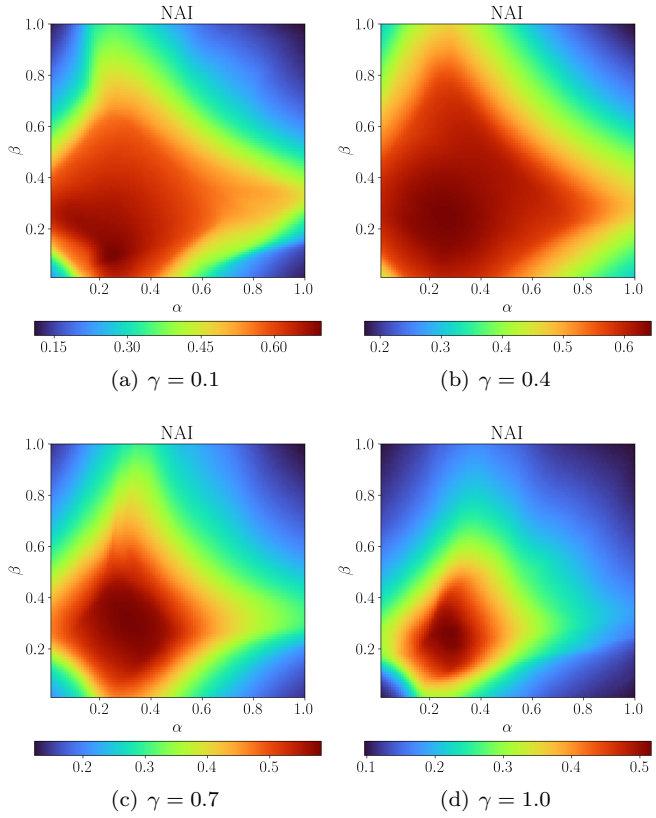

(a) $\gamma = 0.1$ (b) $\gamma = 0.4$

(c) $\gamma = 0.7$ (d) $\gamma = 1.0$

Fig. 15 2D cross-sections of NAI for quadratic Mandelbrot set – varying α, β and fixed γ

low values of α and β. On the other hand, the lowest values of AET are located in the top-right corner. Now, by looking at the NAI plots, we can notice that the dependency is also non-linear. We can see that the biggest Mandelbrot set is obtained for $\gamma = 0.1$ at $\alpha = 0.25$, $\beta = 0.10$, where NAI is equal to 0.69548, i.e., 69% of the area is covered by the set. The lowest NAI value (0.09658) is obtained for $\gamma = 1.0$ at $\alpha = \beta = 1.0$. This value means that 9% of the area is covered by the set. The shapes of the cross-sections are different than those obtained for AET. Moreover, we can observe that the largest sets were obtained for the cross-sections corresponding to lower values of γ. For each cross-section, we see that the smallest sets are obtained in the corners of the parameters' space.

In the second experiment, we generated cross-sections for quartic Mandelbrot sets using γ values: 0.1, 0.4, 0.7, 1.0. The obtained results are presented in Figs. 16–17, and the minimal and maximal values of the numerical measures are gathered in Tab. 2. The AET values vary across the values of γ. The lowest values are obtained for $\gamma = 1.0$, where AET varies between 1.090 (at

Table 1 Minimal and maximal values of AET and NAI computed from Figs. 14–15

γ	min AET (α, β)	max AET (α, β)	min NAI (α, β)	max NAI (α, β)
0.1	2.165	7.195	0.10952	0.69548
	(1.0, 1.0)	(0.08, 0.02)	(1.0, 1.0)	(0.25, 0.10)
0.4	1.842	4.91	0.17434	0.64394
	(1.0, 1.0)	(0.04, 0.01)	(1.0, 1.0)	(0.25, 0.24)
0.7	1.586	4.711	0.12227	0.58288
	(1.0, 1.0)	(0.14, 0.04)	(1.0, 1.0)	(0.31, 0.31)
1.0	1.27	3.637	0.09658	0.51667
	(1.0, 1.0)	(0.14, 0.04)	(1.0, 1.0)	(0.27, 0.26)

$\alpha = \beta = 1.0$) and 2.088 (at $\alpha = 0.05$, $\beta = 0.02$). The values increase with the decrease of γ, obtaining the highest values for $\gamma = 0.1$. For each cross-section, the slowest escape speed of the orbits is obtained for the parameters' values in the neighbourhood of the origin. The dependency in each case is non-linear. The relative set size measured using NAI also depends on α and β in a non-linear way. From the NAI plots, we can observe the concentration of the highest values of this numerical measure in the lower-left quadrant of the parameters' space. The highest values of NAI are obtained for low values of γ, where the maximal value is 0.57776 (at $\alpha = 0.25$, $\beta = 0.18$, $\gamma = 0.1$). This means that the largest set occupies about 57% of the considered area. On the other hand, the smallest set occupies only about 12% of the area (for $\alpha = 0.76$, $\beta = 1.0$, $\gamma = 1.0$).

Table 2 Minimal and maximal values of AET and NAI computed from Figs. 16–17

γ	min AET (α, β)	max AET (α, β)	min NAI (α, β)	max NAI (α, β)
0.1	1.196	4.026	0.13000	0.57776
	(0.98, 1.0)	(0.05, 0.03)	(1.0, 1.0)	(0.25, 0.18)
0.4	1.162	2.974	0.13196	0.50913
	(1.0, 1.0)	(0.08, 0.01)	(1.0, 1.0)	(0.20, 0.22)
0.7	1.228	2.894	0.12328	0.42650
	(1.0, 1.0)	(0.10, 0.01)	(1.0, 1.0)	(0.13, 0.09)
1.0	1.090	2.088	0.12187	0.36684
	(1.0, 1.0)	(0.05, 0.02)	(0.76, 1.0)	(0.08, 0.04)

5.2 Numerical Results for Julia Sets

For obtaining the numerical data for the Julia sets, we used the same values of c, K, and used the same area A as for the graphical examples presented in Sec. 4.2.

To create the cross-sections for the quadratic Julia sets, we used the following γ values: 0.1, 0.4, 0.7, and 1.0. The obtained results of AET and NAI measures are shown in Figs. 18–19, respectively. The maximal and minimal

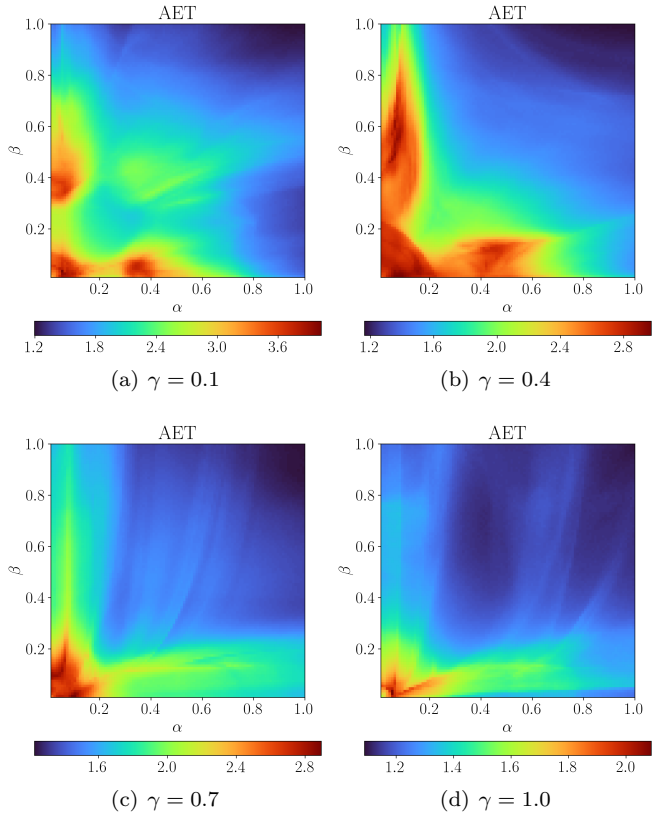

(a) $\gamma = 0.1$ (b) $\gamma = 0.4$

(c) $\gamma = 0.7$ (d) $\gamma = 1.0$

Fig. 16 2D cross-sections of AET for quartic Mandelbrot set – varying α, β and fixed γ

values of both numerical measures are gathered in Tab. 3. When we look at the AET plots in Fig. 18, then we notice that the highest values of this measure are located in the lower-left corner of the parameters' space for the low and mid values of γ. For higher values of γ, we see that the high values are located in the lower half of the parameters' space. We confirm this observation by looking at the maximal values of AET in Tab. 3. From the table, we see that the minimal values of AET increase with the decrease of γ. However, for the maximal values, we do not have such a trend. Each cross-section of AET is a highly non-linear function of the parameters. If we look at the NAI plots, then we also observe a non-linear nature of the dependency. The minimal values for most of the cross-sections are equal to 0.0, which means that in the considered area, there were no points that belong to the filled Julia set. These minimal values are located in the upper-right corner of the parameters space. The maximal values are very high ranging from 0.705 ($\gamma = 1.0$) to 0.990 ($\gamma = 0.1$). The areas of high values of NAI become larger with the decrease of γ, which means that the largest Julia sets are obtained for low values of γ.

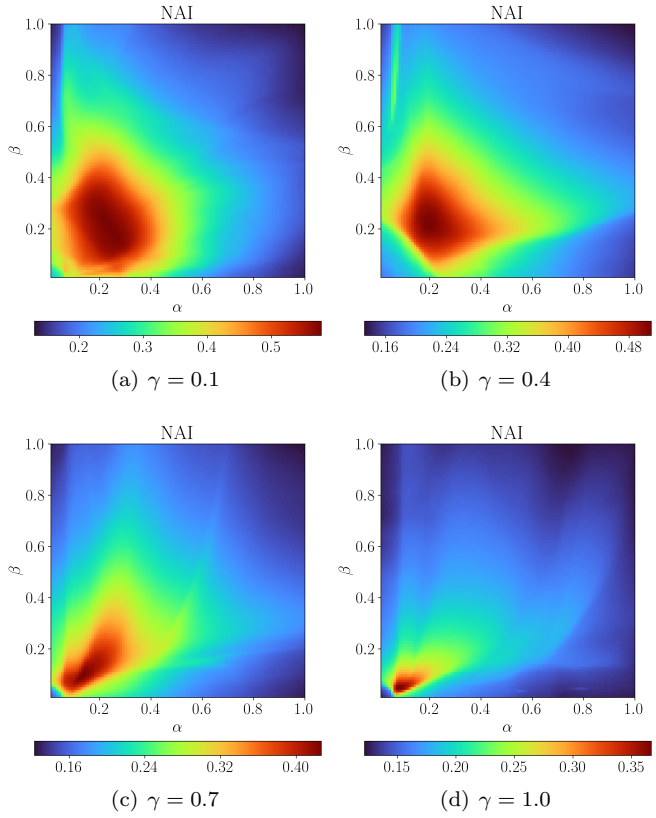

(a) $\gamma = 0.1$ (b) $\gamma = 0.4$

(c) $\gamma = 0.7$ (d) $\gamma = 1.0$

Fig. 17 2D cross-sections of NAI for quartic Mandelbrot set – varying α, β and fixed γ

Table 3 Minimal and maximal values of AET and NAI computed from Figs. 18–19

γ	min AET (α, β)	max AET (α, β)	min NAI (α, β)	max NAI (α, β)
0.1	1.403	6.419	0.00000	0.99073
	(1.00, 1.00)	(0.06, 0.01)	(1.00, 1.00)	(0.13, 0.12)
0.4	1.299	3.479	0.01043	0.89999
	(0.40, 0.78)	(0.10, 0.02)	(1.00, 1.00)	(0.18, 0.28)
0.7	1.092	4.500	0.00000	0.85368
	(1.00, 1.00)	(0.78, 0.16)	(1.00, 1.00)	(0.17, 0.19)
1.0	0.902	3.551	0.00000	0.70584
	(1.00, 1.00)	(0.59, 0.16)	(1.00, 1.00)	(0.15, 0.12)

In our last numerical measurement, we analysed AET and NAI plots for the quartic Julia sets. For this, we used the same values of γ as we used for the quadratic Julia sets, i.e., 0.1, 0.4, 0.7, 1.0. The obtained cross-sections are shown in Figs. 20–21, and the minimal and maximal values of the measures are gathered in Tab. 4. In the AET plots, we can observe an interesting behaviour. The highest values of this measure are located near the axes, forming two

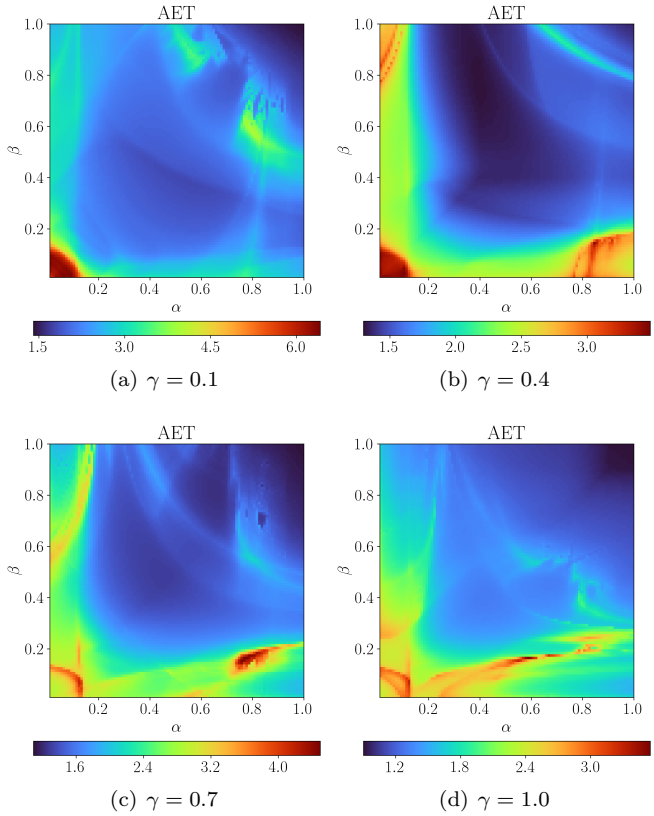

(a) $\gamma = 0.1$ (b) $\gamma = 0.4$

(c) $\gamma = 0.7$ (d) $\gamma = 1.0$

Fig. 18 2D cross-sections of AET for quadratic Julia sets – varying α, β and fixed γ

bands. The first is horizontal, and the second one is vertical. Then, the values decrease as we move away from the axes, obtaining the minimal value near the corner where the two bands join. After reaching the minimal value, the values of AET start to increase. The band size depends on the γ value. Thus, the slowest escape speed is obtained for values of α and β near the axes of the parameters' space. In the case of NAI plots, we do not see a similar behaviour. The highest values of NAI are located near the origin (see Tab. 4). We also see that the minimal and maximal values of NAI increase with the decrease of γ, obtaining the largest sets for low values of γ. The largest set obtained for $\gamma = 0.1$ at $\alpha = 0.12$, $\beta = 0.03$ occupied about 31% of the considered area, whereas the smallest obtained for $\gamma = 1.0$ at $\alpha = 0.99$, $\beta = 1.0$ less than 1%.

6 Conclusions

In the paper, we studied the application of the newly emerging Picard–SP iteration process in the generation of Mandelbrot and Julia sets. We proved

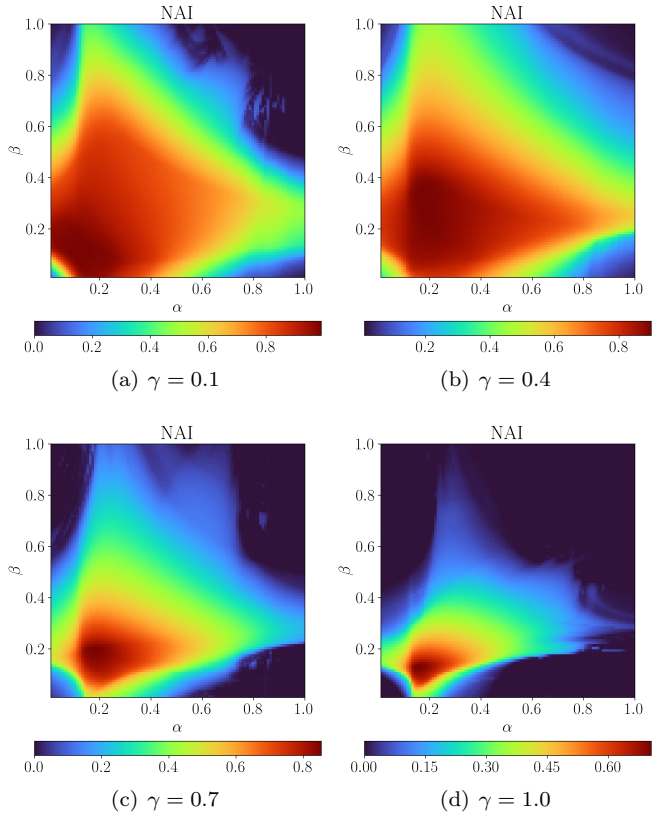

(a) $\gamma = 0.1$ (b) $\gamma = 0.4$

(c) $\gamma = 0.7$ (d) $\gamma = 1.0$

Fig. 19 2D cross-sections of NAI for quadratic Julia sets – varying α, β and fixed γ

Table 4 Minimal and maximal values of AET and NAI computed from Figs. 20–21

γ	min AET (α, β)	max AET (α, β)	min NAI (α, β)	max NAI (α, β)
0.1	0.507	1.287	0.12175	0.31408
	(0.15, 0.10)	(0.03, 0.01)	(1.00, 1.00)	(0.12, 0.03)
0.4	0.135	1.096	0.10997	0.16951
	(0.40, 0.40)	(0.03, 0.01)	(1.00, 1.00)	(0.13, 0.03)
0.7	0.089	1.077	0.08320	0.12703
	(0.70, 0.70)	(0.03, 0.01)	(1.00, 1.00)	(0.14, 0.03)
1.0	0.093	1.672	0.00002	0.10276
	(0.88, 0.88)	(0.59, 0.16)	(0.99, 1.00)	(0.19, 0.04)

an escape criterion for the considered iteration process. Based on the escape criterion, we introduced escape-time algorithms for generating Mandelbrot and Julia sets. Moreover, we examined the relationship between the set size and the parameters of the Picrad–SP orbit using the concept of AET and NAI numerical measures. In each considered example, the dependency was non-trivial and non-linear.

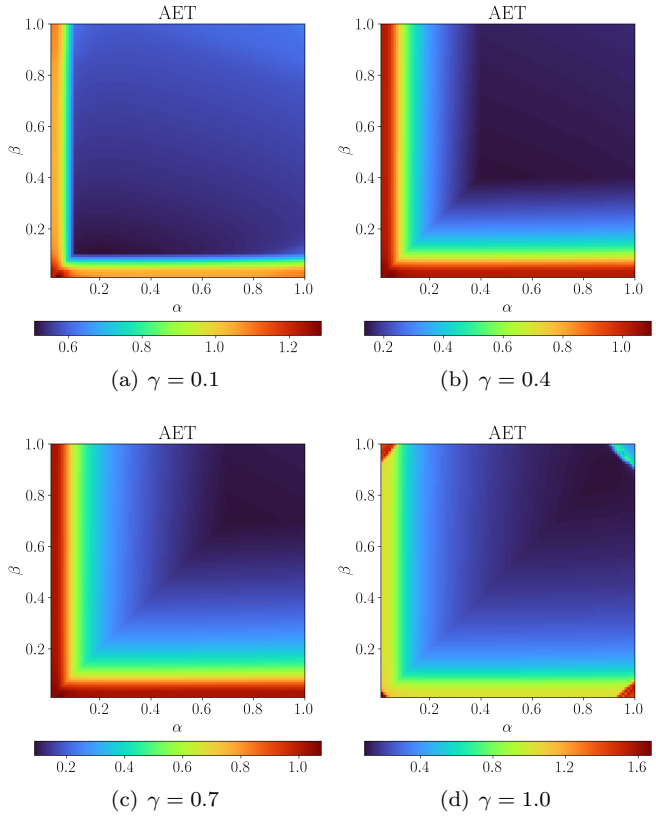

(a) $\gamma = 0.1$ (b) $\gamma = 0.4$

(c) $\gamma = 0.7$ (d) $\gamma = 1.0$

Fig. 20 2D cross-sections of AET for quartic Julia sets – varying α, β and fixed γ

In fixed point theory, we can find various kinds of iteration schemes that can be used with the polynomial map. So, in our future study, we will try to utilize such schemes and study their behaviour. Another direction for future research could be the use of the trinition numbers [6] instead of the complex ones considered in this paper. We can also study the effect of adding noise to the polynomial map analogously like in [1,26].

Data availability

The data that support the findings of this study are available from the corresponding author, upon reasonable request.

Conflicts of interest

The authors declare that they have no conflicts of interest.

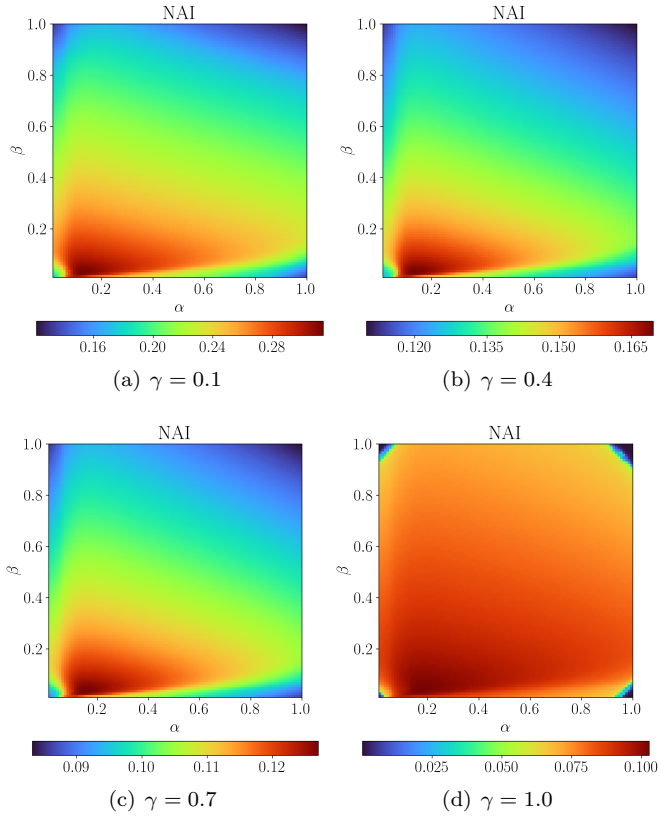

Fig. 21 2D cross-sections of NAI for quartic Julia sets – varying α, β and fixed γ

Funding

No funds were received for this study.

References

1. Agarwal, R., Agarwal, V.: Dynamic noise perturbed generalized superior Mandelbrot sets. Nonlinear Dynamics **67**(3), 1883–1891 (2012). DOI 10.1007/s11071-011-0115-2
2. Agarwal, R., O'Regan, D., Sahu, D.: Iterative construction of fixed points of nearly asymptotically nonexpansive mappings. Journal of Nonlinear and Convex Analysis **8**(1), 61–79 (2007)
3. Amar, A., Jeribi, A., Mnif, M.: Some fixed point theorems and application to biological model. Numerical Functional Analysis and Optimization **29**(1–2), 1–23 (2008). DOI 10.1080/01630560701749482
4. Antal, S., Tomar, A., Prajapati, D., Sajid, M.: Variants of Julia and Mandelbrot sets as fractals via Jungck–Ishikawa fixed point iteration system with *s*-convexity. AIMS Mathematics **7**(6), 10939–10957 (2022). DOI 10.3934/math.2022611
5. Ashish, Rani, M., Chugh, R.: Julia sets and Mandelbrot sets in Noor orbit. Applied Mathematics and Computation **228**, 615–631 (2014). DOI 10.1016/j.amc.2013.11.077

6. Atangana, A., Mekkaoui, T.: Trinition the complex number with two imaginary parts: Fractal, chaos and fractional calculus. Chaos, Solitions & Fractals **128**, 366–381 (2019). DOI 10.1016/j.chaos.2019.08.018
7. Cushing, J., Costantino, R., Dennis, B., Desharnais, R., Henson, S.: Chaos in ecology: experimental nonlinear dynamics. Academic Press (2002)
8. Danet, R.M., Popescu, M.V.: Some applications of the fixed-point theory in economics. Creative Mathematics and Informatics **17**(3), 392–398 (2008)
9. Devaney, R.: A First Course in Chaotic Dynamical Systems: Theory and Experiment, 2nd edn. CRC Press, Boca Raton (2020)
10. Gdawiec, K., Fariello, R., Santos, Y.: On the quaternion Julia sets via Picard–Mann iteration. Nonlinear Dynamics **111**(18), 17591–17603 (2023). DOI 10.1007/s11071-023-08785-0
11. Husain, A., Nanda, M., Chowdary, S., Sajid, M.: Fractals: An eclectic survey, part-i. Fractal and Fractional **6**(2), 89 (2022). DOI 10.3390/fractalfract6020089
12. Husain, A., Nanda, M., Chowdary, S., Sajid, M.: Fractals: An eclectic survey, part ii. Fractal and Fractional **6**(7), 379 (2022). DOI 10.3390/fractalfract6070379
13. Ishikawa, S.: Fixed points by a new iteration method. Proceedings of the American Mathematical Society **44**(1), 147–150 (1974). DOI 10.1090/S0002-9939-1974-0336469-5
14. Julia, G.: Mémoire sur l'itération des fonctions rationnelles. Journal de mathématiques pures et appliquées **8**(1), 47–246 (1918)
15. Kadioglu, N., Yildirim, I.: Approximating fixed points of nonexpansive mappings by a faster iteration process. Journal of Advanced Mathematical Studies **8**(2), 257–264 (2015)
16. Khan, S.: A Picard–Mann hybrid iterative process. Fixed Point Theory and Applications **2013**(1), Article no. 69 (2013). DOI 10.1186/1687-1812-2013-69
17. Kumari, S., Gdawiec, K., Nandal, A., Kumar, N., Chugh, R.: On the viscosity approximation type iterative method and its non-linear behaviour in the generation of Mandelbrot and Julia sets. Numerical Algorithms **96**(1), 211–236 (2024). DOI 10.1007/s11075-023-01644-4
18. Kumari, S., Gdawiec, K., Nandal, A., Postolache, M., Chugh, R.: A novel approach to generate Mandelbrot sets, Julia sets and biomorphs via viscosity approximation method. Chaos, Solitons & Fractals **163**, 112540 (2022). DOI 10.1016/j.chaos.2022.112540
19. Lakhtakia, A., Varadan, V., Messier, R., Varadan, V.: On the symmetries of the Julia sets for the process $z \to z^p + c$. Journal of Physics A: Mathematical and General **20**(11), 3533–3535 (1987). DOI 10.1088/0305-4470/20/11/051
20. Li, D., Tanveer, M., Nazeer, W., Guo, X.: Boundaries of filled Julia sets in generalized Jungck Mann orbit. IEEE Access **7**, 76859–76867 (2019). DOI 10.1109/ACCESS.2019.2920026
21. Mandelbrot, B.: The Fractal Geometry of Nature. W.H. Freeman and Company, San Francisco (1982)
22. Mann, W.: Mean value methods in iteration. Proceedings of the American Mathematical Society **4**(3), 506–510 (1953). DOI 10.1090/S0002-9939-1953-0054846-3
23. Murali, A., Muthunagai, K.: Generation of Julia and Mandelbrot fractals for a generalized rational type mapping via viscosity approximation type iterative method extended with s-convexity. AIMS Mathematics **9**(8), 20221–20244 (2024). DOI 10.3934/math.2024985
24. Nawaz, B., Ullah, K., Gdawiec, K.: Convergence analysis of Picard–SP iteration process for generalized α–nonexpansive mappings. Numerical Algorithms (2024). DOI 10.1007/s11075-024-01859-z. (in press)
25. Nawaz, B., Ullah, K., Gdawiec, K.: Generation of Mandelbrot and Julia sets by using M-iteration process. Chaos, Solitons & Fractals **188**, 115516 (2024). DOI 10.1016/j.chaos.2024.115516
26. Negi, A., Rani, M.: A new approach to dynamic noise on superior Mandelbrot set. Chaos, Solitons & Fractals **36**(4), 1089–1096 (2008). DOI 10.1016/j.chaos.2006.07.026
27. Noor, M.: New approximation schemes for general variational inequalities. Journal of Mathematical Analysis and applications **251**(1), 217–229 (2000). DOI 10.1006/jmaa.2000.7042

28. Picard, E.: Mémoire sur la théorie des équations aux dérivées partielles et la méthode des approximations successives. Journal de Mathématiques pures et appliquées **6**(4), 145–210 (1890)
29. Rana, R., Chauhan, Y., Negi, A.: Non linear dynamics of Ishikawa iteration. International Journal of Computer Applications **7**(13), 43–49 (2010)
30. Rani, M., Kumar, V.: Superior Julia sets. Journal of the Korea Society of Mathematical Education Series D: Research in Mathematical Education **8**(4), 261–277 (2004)
31. Rani, M., Kumar, V.: Superior Mandelbrot set. Journal of the Korea Society of Mathematical Education Series D: Research in Mathematical Education **8**(4), 279–291 (2004)
32. Tassaddiq, A.: General escape criteria for the generation of fractals in extended Jungck–Noor orbit. Mathematics and Computers in Simulation **196**, 1–14 (2022). DOI 10.1016/j.matcom.2022.01.003
33. Tomar, A., Prajapati, D., Antal, S., Rawat, S.: Variants of Mandelbrot and Julia fractals for higher-order complex polynomials. Mathematical Methods in the Applied Sciences (2022). DOI 10.1002/mma.8262. (in press)
34. Ullah, K., Arshad, M.: Numerical reckoning fixed points for Suzuki's generalized nonexpansive mapping's via new iteration process. Filomat **32**(1), 187–196 (2018). DOI 10.2298/FIL1801187U
35. Xiangdong, L., Zhiliang, Z., Guangxing, W., Weiyong, Z.: Composed accelerated escape time algorithm to construct the general Mandelbrot set. Fractals **9**(2), 149–153 (2001). DOI 10.1142/S0218348X01000580
36. Zou, C., Shahid, A., Tassaddiq, A., Khan, A., Ahmad, M.: Mandelbrot sets and Julia sets in Picard–Mann orbit. IEEE Access **8**, 64411–64421 (2020). DOI 10.1109/ACCESS.2020.2984689